

Data analysis of gravitational-wave signals from spinning neutron stars.

IV. An all-sky search

Pia Astone

Istituto Nazionale di Fisica Nucleare, INFN-Rome I, 00185 Rome, Italy

Kazimierz M. Borkowski

Center for Astronomy, Nicolaus Copernicus University, Gagarina 11, 87-100 Toruń, Poland

Piotr Jaranowski

Institute of Theoretical Physics, University of Białystok, Lipowa 41, 15-424 Białystok, Poland

Andrzej Królak

Institute of Mathematics, Polish Academy of Sciences, Śniadeckich 8, 00-950 Warsaw, Poland

(Received 29 December 2000; published 25 January 2002)

We develop a set of data analysis tools for a realistic all-sky search for continuous gravitational-wave signals and we test our tools against simulated data. The aim of the paper is to prepare for an analysis of the real data from the EXPLORER bar detector; however, the methods that we present apply both to data from the resonant bar detectors that are currently in operation and the laser interferometric detectors that are in the final stages of construction and commissioning. With our techniques we shall be able to perform an all-sky coherent search of 2 days of data from the EXPLORER detector for a frequency bandwidth of 0.76 Hz in one month with 250 Mflops computing power. This search will detect all the continuous gravitational-wave signals with the dimensionless amplitude larger than 2.8×10^{-23} with 99% confidence, assuming that the noise in the detector is Gaussian.

DOI: 10.1103/PhysRevD.65.042003

PACS number(s): 95.55.Ym, 04.80.Nn, 95.75.Pq, 97.60.Gb

I. INTRODUCTION AND SUMMARY

It was shown that an all-sky full frequency bandwidth coherent search of data of many months duration for continuous gravitational-wave signals is computationally too prohibitive to be realized with presently available computing power [1,2]. Consequently two alternative approaches emerge. One that we shall call *tracking* involves the tracking of lines in the time-frequency plane built from the Fourier transforms of one day long stretches of data [3,4]. The other that we shall call *stacking* involves dividing the data into day long stretches, searching each stretch for signals, and enhancing the detectability by incoherently summing the Fourier transforms of data stretches [5]. In this paper we develop data analysis tools for the first stage of the stacking approach, namely for the coherent search of a few days long stretches of data. These tools involve storage of the data in the Fourier domain database, calculation of the precise position of the detector with respect to the solar system barycenter using JPL ephemeris, calculation of the detection thresholds, approximation of the signal by a simple linear model, and construction of the grid of templates in the parameter space ensuring that the loss of signals due to the finite spacing of the grid is minimized.

In this theoretical work we have in mind a particular set of data, namely the data collected by the EXPLORER bar detector. This detector is most sensitive over certain two narrow bandwidths of about 1 Hz wide at a frequency around 1 kHz. To make the search computationally feasible we propose an all-sky search of a few days long stretches of data in the narrow band where the detector has the best sensitivity.

We find that with 250 Mflops of computing power we can carry out a complete all-sky search in around a month for signals within a bandwidth of 0.76 Hz at a frequency of 922 Hz and for observation time of 2 days. We assume that the minimum characteristic time for the change of the signal's frequency is 1000 years. By our search we shall be able to detect all the continuous gravitational-wave signals with the parameters given above and with the dimensionless amplitude larger than 2.8×10^{-23} with 99% confidence.

The tools developed in this work can be applied not only to the analysis of the bar data but also to the interferometer data. In the case of the wide-band interferometer one can divide the data into many narrow bands and analyze each band using the algorithms presented in this paper.

The plan of the paper is as follows. In Sec. II we present responses of a laser interferometer and a resonant bar to a continuous gravitational wave, including the effects of both amplitude and frequency modulation of the response. The optimal data processing method is described in Sec. III. In Sec. IV we introduce the frequency domain database and in Sec. V we discuss how to calculate the precise position of the detector with respect to the solar system barycenter. In Sec. VI we introduce an approximate model of the detector's response called the linear model and we describe its performance. In Sec. VII we construct a grid of templates in the parameter space, we calculate the computational requirements to do the search, and we perform Monte Carlo simulations to test the performance of our grid and our search algorithm. In Sec. VIII we discuss and choose parameters for our planned all-sky search of the EXPLORER detector data. Several details are presented in the Appendixes.

Many methods presented in this paper rely on general analytic tools developed in a previous paper of this series [6] that we shall call Paper III.

II. DETECTOR'S NOISE-FREE RESPONSE

Dimensionless noise-free response function h of the gravitational-wave detector to a weak plane gravitational wave in the long wavelength approximation [i.e., when the size of the detector is much smaller than the reduced wavelength $\lambda/(2\pi)$ of the wave] can be written as a linear combination of the wave polarization functions h_+ and h_\times :

$$h(t) = F_+(t)h_+(t) + F_\times(t)h_\times(t), \quad (2.1)$$

where F_+ and F_\times are called the beam-pattern functions. Explicit formulas for the interferometric and the bar beam-pattern functions can be found in Appendix A, where we have also included the derivation of the beam-pattern functions for the bar detector.

We are interested in a continuous gravitational wave described by the wave polarization functions of the form

$$h_+(t) = h_{0+} \cos \Psi(t), \quad (2.2a)$$

$$h_\times(t) = h_{0\times} \sin \Psi(t), \quad (2.2b)$$

where h_{0+} and $h_{0\times}$ are the amplitudes of the two independent wave polarizations, Ψ is the phase of the wave. The amplitudes h_{0+} and $h_{0\times}$ depend on the physical mechanisms generating the gravitational wave. In the case of a wave originating from a spinning neutron star which possesses some static deviation from axisymmetry (supported by the solid crust or by the star's own magnetic field) these amplitudes can be estimated by

$$h_0 = 4.23 \times 10^{-23} \left(\frac{\epsilon}{10^{-5}} \right) \left(\frac{I}{10^{45} \text{ g cm}^2} \right) \left(\frac{1 \text{ kpc}}{r} \right) \left(\frac{f}{1 \text{ kHz}} \right)^2, \quad (2.3)$$

where I is the neutron star moment of inertia with respect to the rotation axis, ϵ is the gravitational ellipticity of the star, r is the distance to the star, and f the frequency of the gravitational wave. The value of 10^{-5} of the parameter ϵ in the above estimate should be treated as an upper bound. In reality it may be several orders of magnitude less. A different mechanism, such as the Chandrareskhar-Friedman-Schutz instability, would give a different dependence of the amplitude on the frequency of the wave.

The phase Ψ of the wave is given by

$$\Psi(t) = \Phi_0 + \Phi(t), \quad (2.4a)$$

$$\Phi(t) = \sum_{k=0}^{s_1} \omega_k \frac{t^{k+1}}{(k+1)!} + \frac{\mathbf{n}_0 \cdot \mathbf{r}_{\text{SSB}}(t)}{c} \sum_{k=0}^{s_2} \omega_k \frac{t^k}{k!}, \quad (2.4b)$$

where Φ_0 is the initial phase of the wave form, \mathbf{r}_{SSB} is the vector joining the solar system barycenter (SSB) with the detector, and \mathbf{n}_0 is the constant unit vector in the direction from the SSB to the neutron star. We assume that the gravi-

tational wave form is almost monochromatic around some angular frequency ω_0 which we define as the instantaneous angular frequency evaluated at the SSB at $t=0$, and ω_k ($k=1,2,\dots$) is the k th time derivative of the instantaneous angular frequency at the SSB evaluated at $t=0$. To obtain formulas (2.4), we model the frequency of the signal in the rest frame of the neutron star by a Taylor series. For the detailed derivation of the phase model (2.4) see Sec. II B and Appendix A of Ref. [2]. The integers s_1 and s_2 are the number of spin downs to be included in the two components of the phase. We need to include enough spin downs so that we have a sufficiently accurate model of the signal to extract it from the noise. This will depend on the length of the observation time.

It is convenient to decompose the response h of the gravitational-wave detector (both resonant bar and laser interferometer) described by Eqs. (2.1), (2.2), and (2.4) [cf. also Eqs. (A1) and (A10) in Appendix A] into a linear combination of several components:

$$h(t) = \sum_{i=1}^4 A_i h_i(t), \quad (2.5)$$

where the four constant amplitudes A_i are given by

$$A_1 = \sin \zeta (h_{0+} \cos 2\psi \cos \Phi_0 - h_{0\times} \sin 2\psi \sin \Phi_0), \quad (2.6a)$$

$$A_2 = \sin \zeta (h_{0\times} \cos 2\psi \sin \Phi_0 + h_{0+} \sin 2\psi \cos \Phi_0), \quad (2.6b)$$

$$A_3 = \sin \zeta (-h_{0+} \cos 2\psi \sin \Phi_0 - h_{0\times} \sin 2\psi \cos \Phi_0), \quad (2.6c)$$

$$A_4 = \sin \zeta (h_{0+} \cos 2\psi \cos \Phi_0 - h_{0\times} \sin 2\psi \sin \Phi_0). \quad (2.6d)$$

The amplitudes A_i depend, through h_{0+} and $h_{0\times}$, on the physical mechanism generating the gravitational wave. They also depend on the initial phase Φ_0 of the wave form and the polarization angle ψ of the wave. The angle ζ is the angle between the interferometer arms (usually $\zeta=90^\circ$), and for the case of bars always $\zeta=90^\circ$.

The functions h_i do not depend on the mechanism generating the gravitational wave and they have the form

$$h_1(t) = a(t) \cos \Phi(t), \quad (2.7a)$$

$$h_2(t) = b(t) \cos \Phi(t), \quad (2.7b)$$

$$h_3(t) = a(t) \sin \Phi(t), \quad (2.7c)$$

$$h_4(t) = b(t) \sin \Phi(t), \quad (2.7d)$$

where the amplitude modulation functions a and b can be found in Appendix A [see Eqs. (A2) for an interferometer and Eqs. (A11) for a bar], and Φ is the phase given by Eq. (2.4b). The functions a and b depend on the right ascension α and the declination δ of the source (they also depend on the detector's geodetic latitude ϕ and the angle γ describing the orientation of the detector with respect to local geo-

graphical directions). The phase Φ depends on the angular frequency ω_0 , s spin-down parameters ω_k ($k=1,\dots,s$), and on the angles α , δ ; it also depends on the latitude ϕ of the detector. We call parameters ω_0 , ω_k , α , δ the phase parameters. The whole signal h depends thus on $s+5$ unknown parameters: h_{0+} , $h_{0\times}$, α , δ , ω_0 , and ω_k .

The amplitude modulation, determined by the functions a and b , splits the power spectrum of the signal into five lines corresponding to angular frequencies $\omega_0-2\Omega_r$, $\omega_0-\Omega_r$, ω_0 , $\omega_0+\Omega_r$, and $\omega_0+2\Omega_r$, where Ω_r is the rotational angular velocity of the Earth. Moreover, the maximum of the signal's power can be in any of these components depending on the position of the source in the sky. Therefore we need to take the amplitude modulation into account in the design of a matched filter since a filter of constant amplitude and matched only to the phase would mean a drastic decrease of the signal-to-noise ratio.

III. OPTIMAL DATA ANALYSIS METHOD

The signal given by Eq. (2.5) will be buried in the noise of a detector. Thus we are faced with the problem of detecting the signal and estimating its parameters. A standard method is the method of maximum likelihood (ML) detection that consists of maximizing the likelihood function, which we shall denote by Λ , with respect to the parameters of the signal. If the maximum of Λ exceeds a certain threshold calculated from the false alarm probability that we can afford, we say that the signal is detected. The values of the parameters that maximize Λ are said to be the maximum likelihood estimators of the parameters of the signal. The magnitude of the maximum of Λ determines the probability of detection of the signal.

In the current paper we consider the gravitational-wave signal consisting of one narrow-band component. The ML detection of a more general signal consisting of N narrow-band components was studied in detail in Sec. III of Paper III. We only need here to recall the main results derived in Paper III and specialize them to the case of a one-component signal. A related approach to signal detection has also been developed by Owen [7], Mohanty and Dhurandhar [8], and Mohanty [9].

We assume that the noise in the detector is an additive, stationary, Gaussian, and zero-mean continuous random process. We also assume that over the frequency bandwidth of the signal the (one-sided) noise spectral density $S_h(f)$ is nearly constant and equal to $S_h(f_0)$, where f_0 is the frequency of the signal measured at the SSB at $t=0$. Moreover, to simplify analytic formulas, we are restricted to the observation time T_o being an integer multiple of one sidereal day, i.e., $T_o = n(2\pi/\Omega_r)$ for some positive integer n . Then the analytic formulas for the ML estimators of the amplitudes A_i , cf. Eq. (2.5), are given by (for derivation, cf. Sec. III A of Paper III)

$$\hat{A}_1 \approx 2 \frac{\langle xh_1 \rangle}{\langle a^2 \rangle}, \quad (3.1a)$$

$$\hat{A}_2 \approx 2 \frac{\langle xh_2 \rangle}{\langle b^2 \rangle}, \quad (3.1b)$$

$$\hat{A}_3 \approx 2 \frac{\langle xh_3 \rangle}{\langle a^2 \rangle}, \quad (3.1c)$$

$$\hat{A}_4 \approx 2 \frac{\langle xh_4 \rangle}{\langle b^2 \rangle}, \quad (3.1d)$$

where we have introduced the following notation (here $[0, T_o]$ is the observation interval):

$$\langle x \rangle := \frac{1}{T_o} \int_0^{T_o} x(t) dt. \quad (3.2)$$

Explicit formulas for the time averages $\langle a^2 \rangle$ and $\langle b^2 \rangle$ are given in Appendix B.

The reduced logarithmic likelihood function \mathcal{F} can be written as¹

$$\mathcal{F} \approx \frac{2}{S_h(f_0)T_o} \left(\frac{|F_a|^2}{\langle a^2 \rangle} + \frac{|F_b|^2}{\langle b^2 \rangle} \right), \quad (3.3)$$

where

$$F_a := \int_0^{T_o} x(t) a(t) \exp[-i\Phi(t)] dt, \quad (3.4a)$$

$$F_b := \int_0^{T_o} x(t) b(t) \exp[-i\Phi(t)] dt. \quad (3.4b)$$

Thus the ML detection in Gaussian noise leads to a matched filter. The ML estimators of the signal's parameters are obtained in two steps. Firstly, the estimators of the frequency, the spin-down parameters, and the angles α and δ are obtained by maximizing the functional \mathcal{F} with respect to these parameters. Secondly, the estimators of the amplitudes A_i are calculated from the analytic formulas (3.1) with the correlations $\langle xh_i \rangle$ evaluated for the values of the parameters obtained in the first step. Thus filtering for the narrow-band gravitational-wave signal requires two linear complex filters.

When the signal is absent and phase parameters are known $2\mathcal{F}$ has a χ^2 distribution with four degrees of freedom and when the signal is present it has a noncentral χ^2 distribution with four degrees of freedom and noncentrality parameter equal to the optimal signal-to-noise ratio d . When phase parameters are unknown we can approximate \mathcal{F} by a homogeneous χ^2 random field and divide the parameter space into elementary cells defined by the correlation function of \mathcal{F} (consult Sec. III B of Paper III for details). The false alarm probability, i.e., the probability P_F^T that \mathcal{F} exceeds the threshold \mathcal{F}_0 in *one or more* cells is given by

$$P_F^T(\mathcal{F}_0) = 1 - [1 - P_F(\mathcal{F}_0)]^{N_c}, \quad (3.5)$$

¹ \mathcal{F} is the logarithmic likelihood function Λ with amplitudes A_i replaced by their ML estimators \hat{A}_i .

where N_c is the total number of elementary cells and

$$P_F(\mathcal{F}_0) = (1 + \mathcal{F}_0) \exp(-\mathcal{F}_0). \quad (3.6)$$

The expected number of false alarms N_F is given by

$$N_F = N_c P_F(\mathcal{F}_0). \quad (3.7)$$

The probability of detection P_D , i.e., the probability that \mathcal{F} exceeds the threshold \mathcal{F}_0 when the signal-to-noise ratio is equal to d is given by

$$P_D(d, \mathcal{F}_0) = \int_{\mathcal{F}_0}^{\infty} p_1(d, \mathcal{F}) d\mathcal{F}, \quad (3.8)$$

where

$$p_1(d, \mathcal{F}) = \frac{\sqrt{2\mathcal{F}}}{d} I_1(d\sqrt{2\mathcal{F}}) \exp\left(-\mathcal{F} - \frac{1}{2}d^2\right). \quad (3.9)$$

Here I_1 is the modified Bessel function of the first kind and order 1.

It will very often be the case that the filter we use to extract the signal from the noise is not optimal. This may be the case when we do not know the exact form of the signal (this is almost always the case in practice) or we choose a suboptimal filter to reduce the computational cost and simplify the analysis. For such a case in Sec. VI of Paper III we have developed a theory of suboptimal filtering. The suboptimal statistics \mathcal{F}_{sub} has the same form as the optimal statistics \mathcal{F} and the data analysis procedure consists of maximizing the value of the suboptimal statistics. One can show that

$$E_1\{\mathcal{F}_{\text{sub}}\} = 1 + \frac{1}{2}d_{\text{sub}}^2, \quad (3.10)$$

where E_1 is the expectation value when the signal is present and the parameter d_{sub} is the suboptimal signal-to-noise ratio.

The formulas for the false alarm and detection probabilities have the same form as in the case of the optimal filter except that the optimal signal-to-noise ratio is replaced by the suboptimal one. Also for the suboptimal filter the number of cells N_{sc} may be different than for the optimal one. Thus the false alarm probability is given by

$$P_{sF}^T(\mathcal{F}_0) = 1 - [1 - P_F(\mathcal{F}_0)]^{N_{sc}}. \quad (3.11)$$

The expected number of false alarms N_{sF} reads

$$N_{sF} = N_{sc} P_{sF}(\mathcal{F}_0). \quad (3.12)$$

The detection probability takes the form

$$P_D(d_{\text{sub}}, \mathcal{F}_0) = \int_{\mathcal{F}_0}^{\infty} p_1(d_{\text{sub}}, \mathcal{F}) d\mathcal{F}, \quad (3.13)$$

where the probability density function p_1 is given by Eq. (3.9). Equation (3.10) implies that maximizing the expectation value of the suboptimal statistics when the signal is present is equivalent to maximizing suboptimal signal-to-

noise ratio. We can identify the maximum $d_{s \text{ max}}$ of d_{sub} as the signal-to-noise ratio of the suboptimal filter. It was shown in Paper III that

$$d_{s \text{ max}} = \text{FF}d, \quad (3.14)$$

where FF is the fitting factor introduced by Apostolatos [10]. The fitting factor FF between a signal $h(t; \theta)$ and a filter $h'(t; \theta')$ (θ and θ' are the parameters of the signal and the filter, respectively) is defined as²

$$\text{FF} := \max_{\theta'} \frac{(h(t; \theta) | h'(t; \theta'))}{\sqrt{(h(t; \theta) | h(t; \theta))} \sqrt{(h'(t; \theta') | h'(t; \theta'))}}. \quad (3.15)$$

The fitting factor is a good measure of the quality of the suboptimal filter; however, the performance of the filter can only be fully determined by the false alarm and detection probabilities given by Eqs. (3.11) and (3.13).

IV. THE FREQUENCY DOMAIN DATABASE

The data collected by the detector constitute a time series with a sampling interval Δt . This time domain sequence can also be stored in the frequency domain without any loss of information. Organization of the data in the frequency domain in a suitable way provides a very flexible database that is very useful both for search of the data for gravitational-wave signals and for characterization of the noise of the detector. The first step in constructing a frequency domain database consists simply of taking a fast Fourier transform (FFT) of $2N$ data points and storing the first N points of the FFT. To improve the quality of the time-domain data that will eventually be extracted from the database the original data are windowed and overlapped. Each FFT is then normalized and calibrated where the calibration process takes into account the transfer function of the detector so that the units of the FFT are strain/ $\sqrt{\text{Hz}}$. Moreover, the quality of the data represented by the FFT is characterized so that it is possible to choose thresholds for vetoing the data or criteria to weight them. Both the calibration and the data characterization information are stored in the header that is attached to each FFT.

It is very important to choose a suitable number N of data in each FFT. This depends on the type of signal search that one wants to perform. In the case of the search for continuous sources, which is a subject of this work, we choose N in such a way the maximum expected Doppler shift due to the motion of the detector with respect to SSB is less than the width of one bin. In the case of the EXPLORER data this leads to $N = 2^{16}$. For sampling time $\Delta t = 0.18176 \text{ s}$ this means the length of data for each FFT of around two-thirds of an hour. Another important criterion for the choice of the length of data interval for each FFT is that within the interval the noise is stationary. In the case of the EXPLORER detec-

²For the narrow-band signals considered in our paper the scalar product $(h|h')$ can be approximated as $(h|h') \approx [2/S_h(f_0)] \int_0^{T_0} h(t) h'(t) dt$.

tor stationarity is in general preserved over two-thirds of an hour intervals.

The detailed steps to create the frequency domain database and to extract narrow-band time series from the base are given in Ref. [11].

V. POSITION AND VELOCITY OF THE DETECTOR WITH RESPECT TO THE SOLAR SYSTEM BARYCENTER

A. Dealing with time scales

The data acquisition system of the detector is synchronized to the coordinated universal time (UTC) as disseminated by international time services. Thus it is assumed that each datum corresponds to a given UTC. The UTC scale is essentially uniform, except for occasional 1 s steps introduced internationally to compensate for the variable Earth rotation. When these steps are taken into account, the UTC is reduced to the international atomic time (TAI) scale, which is uniform and differs from the terrestrial dynamical time (TDT) (or TT, normally used to describe celestial phenomena by astronomers) only by a constant term. In principle, the time argument of positions of celestial objects is the barycentric dynamical time (TDB); however, it differs from the TDT only by a very small additive term (less than 0.001 s in magnitude), thus for all practical purposes they do not have to be distinguished. So we have

$$\text{TDB} \approx \text{TDT} = \text{TAI} + 32.184 \text{ s},$$

where TAI is obtained from UTC by removing the time steps.³ One can thus relate given UTC with barycentric positions of all the major celestial bodies of the solar system.

However, to relate the position of a point on Earth to the barycenter of Earth (the latter being obtained from the solar system ephemeris) one has to use yet another time scale—the rotational time scale UT1, which is nonuniform and is determined from astronomical observations. The difference UT1–UTC, which is maintained within ± 0.90 s, is taken from the International Earth Rotation Service (IERS) tabulations of daily values.⁴

B. Topocentric coordinates

To be able to relate a point on Earth's surface to the solar system barycenter it is necessary to know the orientation of Earth in space. The primary effects that should be taken into account are diurnal (variable) rotation, precession and nutation of Earth's rotational axis, and polar motion. The precession and nutation can be accounted for by applying standard astronomical theories. The remaining two effects are unpredictable for a longer future, so observational data must be used.⁵

³The time steps are available in the form of a table; see <http://hpiers.obspm.fr/webiers/general/earthor/utc/table1.html>.

⁴They are available as eopc04.yy files, where “yy” stands for a two digit year number (e.g., “99” for 1999, and “00” for 2000); see <http://hpiers.obspm.fr/iers/eop/eopc04>.

⁵For past years, since 1962, the data necessary for reduction are included in eopc04.yy files mentioned in footnote 4.

The polar motion is taken into account by modifying the conventional geographical coordinates of a point on Earth:

$$\phi = \phi_0 + P_x \cos \lambda_0 - P_y \sin \lambda_0, \quad (5.1a)$$

$$\lambda = \lambda_0 + (P_x \sin \lambda_0 + P_y \cos \lambda_0) \tan \phi_0, \quad (5.1b)$$

where ϕ_0 is the conventional geographical latitude, λ_0 is the conventional longitude, and P_x and P_y are the coordinates of the pole with respect to the conventional international origin.

The rotational angle of Earth is included through conversion of UTC to UT1 (the quantity UT1–UTC is tabulated in the IERS files). UT1 serves to calculate the apparent sidereal time θ , which is essentially equal to $\phi_r + \Omega_r t$ of Eqs. (A2) and (A11) plus the nutation in longitude projected on the celestial equator. The sidereal time in turn is used to find rectangular coordinates of the point (the detector) in the IERS celestial reference frame:

$$x_E = r \cos \theta, \quad (5.2a)$$

$$y_E = r \sin \theta, \quad (5.2b)$$

$$z_E = b \sin \psi + h \sin \phi, \quad (5.2c)$$

where

$$r = a \cos \psi + h \cos \phi \quad (5.3)$$

is the equatorial component of the radius vector, $\psi = \arctan(b \tan \phi/a)$ is the reduced latitude, h is the height above Earth's ellipsoid, and $a = 6378.140$ km and $b = a(1 - 1/f)$ (where $f = 298.257$) are the semiaxes of Earth's ellipsoid. These coordinates are affected by the polar motion through dependence of r and ψ on ϕ , and θ on λ .

The polar motion (P_x and P_y) and UT1–UTC quantities are linearly interpolated between the daily IERS values.

Since these coordinates are naturally referred to the epoch of date, they are further precessed back to the standard epoch J2000. The precessed Cartesian coordinates $(x_E, y_E, z_E)_{2000}$ may now be straightforwardly added to coordinates of Earth's barycenter with respect to the solar system barycenter (which are described in the next paragraph) to obtain the desired position vector of the detector.

C. Barycentric coordinates of the Earth (JPL ephemeris)

For computing the coordinates of Earth's barycenter, relative to the SSB, use is made of the latest JPL Planetary and Lunar Ephemerides, “DE405/LE405” or just “DE405”,⁶ created in 1997 and described in detail by Standish [12]. It represents an improvement over its predecessor, DE403. DE405 is based upon the international celestial reference frame (ICRF) (an earlier popular ephemeris DE200, which has been the basis of the *Astronomical Alma-*

⁶It is available via the Internet (anonymous ftp: navigator.jpl.nasa.gov, the directory: ephem/export) or on CD (from the publisher: Willmann-Bell, Inc., <http://www.willbell.com/software/jpl.htm>).

nac since 1984, is within 0.01 arcsec of the frame of the ICRF). It consists of a set of Chebyshev polynomials fit with full precision to a numerical integration from 1600 AD to 2200 AD. Over this interval the interpolating accuracy is not worse than 25 m for any planet and not worse than 1 m for the Moon. The JPL package allows a professional user to obtain the rectangular coordinates of the Sun, Moon, and nine major planets anywhere between JED 2305424.50 (1599 Dec. 09) to JED 2525008.50 (2201 Feb. 20).

In the application described in this paper we have used only a 21-year (1990 to 2010) subset of the original ephemeris. The ephemeris gives separately the position of the Earth-Moon barycenter and the Moon's position relative to this barycenter. The Earth position vector is thus calculated as a fraction (involving the masses of the two bodies) of the Moon's one and opposite for the latter.

Finally, the vector traveled by the Sun towards its apex (with the speed of 20 km/s) between J2000 and the epoch of observation is added to Earth's barycentric position. The direction of the solar apex is assumed at 18^h in right ascension and 30° in declination at the epoch J1900. This direction is precessed to J2000. What is commonly known as the solar apex refers rather to the solar system barycenter apex. However, since the apex motion is known only approximately, really there is no need to distinguish between motions of the Sun and of the barycenter.

D. Velocities

Although the primary concern in this project is to convert positions, the velocity of the gravitational-wave detector relative to the SSB may prove to be useful in future analyses of spectra obtained from the acquired data.

The velocity of the detector is the sum of the diurnal rotational motion of Earth, Earth's motion in space relative to the SSB, and the motion of the solar system itself towards the apex. The last of the named components, towards the apex, has been described in the previous paragraph. The Earth barycentric velocity vector is obtained directly from the JPL ephemeris along with the position vector. Finally, the detector motion relative to Earth's barycenter is represented by a vector of constant length $v_0 := 2\pi r/(\text{sidereal day})$ directed always towards the east in the topocentric reference frame. Thus this diurnal velocity vector has the following Cartesian components (in the barycentric reference frame):

$$V_x = v_0 \cos(\theta + \pi/2), \quad (5.4a)$$

$$V_y = v_0 \sin(\theta + \pi/2), \quad (5.4b)$$

$$V_z = 0. \quad (5.4c)$$

This vector is rotated back to J2000 by the precessional angle.

A short description of the FORTRAN code that generates both the position and the velocity of a detector with respect to the SSB is given in Appendix C.

VI. A LINEAR FILTER

The phase of the gravitational-wave signal contains terms arising from the motion of the detector with respect to the SSB. These terms consist of two contributions, one which comes from the motion of the Earth barycenter with respect to the SSB, and the other which is due to the diurnal motion of the detector with respect to Earth's barycenter. The first contribution has a period of one year and thus for shorter observation times can be well approximated by a few terms of the Taylor expansion. The second term has a period of one sidereal day and to a very good accuracy can be approximated by a circular motion. We thus propose the following *approximate* simple model of the phase of the gravitational-wave signal;

$$\Psi_s(t) = p + p_0 t + \sum_{k=1}^s p_k t^{k+1} + A \cos(\Omega_r t) + B \sin(\Omega_r t), \quad (6.1)$$

where Ω_r is the rotational angular velocity of Earth. The parameters A and B can be related to the right ascension α and the declination δ of the gravitational-wave source through the equations [cf. Eq. (18) in Ref. [2]]

$$A = \frac{\omega_0 r}{c} \cos \delta \cos(\alpha - \phi_r), \quad (6.2a)$$

$$B = \frac{\omega_0 r}{c} \cos \delta \sin(\alpha - \phi_r), \quad (6.2b)$$

where ω_0 is the angular frequency of the gravitational-wave signal and r is defined in Eq. (5.3).

The phase model (6.1) has the property that it is a linear function of the parameters. We have shown in Paper III that for linear phase models the optimal statistics is a homogeneous random field and consequently the statistical theory of signal detection described in Sec. III of the present paper applies to this case. The polynomial in the time part of the phase Ψ_s [cf. Eq. (6.1)] contains two contributions. The first one comes from the intrinsic frequency drift of the gravitational waves emitted by a source. For example, if the source is a spinning neutron star, the frequency of the gravitational waves it emits can evolve as the frequency of the revolution of the star. In general the star will lose its energy and will spin down. This evolution of the frequency can be approximated by a Taylor series. The second contribution comes from the Taylor expansion of the motion of the Earth around the Sun. It is clear that the longer the observation time of the signal the more terms of the Taylor expansion we need to include in order to accurately approximate the true signal.

In order to verify the accuracy of the linear model (6.1) we have calculated the fitting factor (FF) between the linear model and the accurate model of the signal. As the accurate model of the phase of the signal we have taken the following model:

$$\Psi_a(t) = \Phi_0 + \omega_d t + \sum_{k=1}^{s+1} \omega_k t^{k+1} + \left[\omega_0 + \sum_{k=1}^{s+1} (k+1) \omega_k t^k \right] \frac{\mathbf{n}_0 \cdot \mathbf{r}_{\text{SSB}}(t)}{c}, \quad (6.3)$$

where ω_d is the signal's frequency ω_0 shifted by a *known* frequency ω_s , i.e., $\omega_d = \omega_0 - \omega_s$. The down-conversion frequency ω_s (as well as the bandwidth of the signal) can be chosen arbitrarily and an appropriate time sequence can be extracted from the frequency domain database as described in Ref. [11]. The parameters ω_k are spin-down parameters and they arise by approximating the intrinsic frequency evolution of the signal by a Taylor expansion. In the accurate model (6.3) we include one more spin down than in the linear model (6.1). This additional spin down serves to represent the uncertainty of our model.

For the case when the signal is narrow band around some frequency ω_0 the formula (3.15) for the fitting factor can be approximated by

$$\text{FF} \approx \max_{\zeta} \langle \cos[\Psi_a(t; \zeta_a) - \Psi_s(t; \zeta)] \rangle, \quad (6.4)$$

where $\zeta_a = (\Phi_0, \omega_0, \omega_1, \dots, \omega_{s+1}, \alpha, \delta)$ are the parameters of the accurate model (6.3) and $\zeta = (p, p_0, p_1, \dots, p_s, A, B)$ are the parameters of the linear model (6.1). The linear phase model (6.1) can shortly be written as

$$\Psi_s(t; \zeta) = \sum_{i=0}^{s+3} \zeta_i l_i(t). \quad (6.5)$$

The phase Ψ_a in the accurate model (6.3) can be expressed as a sum similar to the sum from Eq. (6.5) plus a certain remainder r that we assume to be small:

$$\Psi_a(t; \zeta_a) = \sum_{i=0}^{s+3} \bar{\zeta}_{ai}(\zeta_a) l_i(t) + r(t; \zeta_a). \quad (6.6)$$

Note that the coefficients $\bar{\zeta}_{ai}$ are some functions of the accurate phase parameters ζ_a . In numerical calculations described below the vector \mathbf{r}_{SSB} in the accurate phase model (6.3) was computed by our TOP2BARY code described in Appendix C, and then the coefficients $\bar{\zeta}_{ai}$ and the residual $r(t; \zeta_a)$ were computed by making a least-squares fit (within the observational interval) of the template $\sum_i \bar{\zeta}_{ai} l_i(t)$ to the accurate phase $\Psi_a(t; \zeta_a)$.

Making use of Eqs. (6.5) and (6.6), from Eq. (6.4) one gets

$$\begin{aligned} \text{FF} &\approx \max_{\zeta} \left\langle \cos \left[\sum_{i=0}^{s+3} (\bar{\zeta}_{ai} - \zeta_i) l_i(t) + r(t) \right] \right\rangle \\ &\approx \max_{\zeta} \left\langle \left[1 - \frac{1}{2} \sum_{i,j=0}^{s+3} (\bar{\zeta}_{ai} - \zeta_i)(\bar{\zeta}_{aj} - \zeta_j) l_i(t) l_j(t) \right] \right. \\ &\quad \left. \times \cos r(t) - \sum_{i=0}^{s+3} (\bar{\zeta}_{ai} - \zeta_i) l_i(t) \sin r(t) \right\rangle, \quad (6.7) \end{aligned}$$

where the last approximation was obtained by Taylor expansion of the cosine function and by keeping only the quadratic terms in the (assumed to be small) differences $\bar{\zeta}_{ai} - \zeta_i$. It is now easy to find in Eq. (6.7) the maximum over the parameters ζ as the right-hand side of Eq. (6.7) is quadratic in these parameters. The values of the parameters that maximize the fitting factor are given by the solution of the following set of $s+4$ linear equations:

$$\sum_{j=0}^{s+3} L_{ij} (\bar{\zeta}_{aj} - \zeta_j) = -L_i, \quad (6.8)$$

where

$$L_{ij} := \langle l_i(t) l_j(t) \cos r(t) \rangle, \quad (6.9a)$$

$$L_i := \langle l_i(t) \sin r(t) \rangle. \quad (6.9b)$$

We have used the above prescription to calculate the fitting factor numerically. Once we have found the parameters of the extremum (6.7) by solving Eqs. (6.8), we have used these values as input to an optimization routine (based on the Nelder-Mead simplex algorithm) to find an accurate value of the fitting factor directly from the formula (6.4) without the Taylor expansion. The Nelder-Mead method is one of the algorithms to find extremum of a function of n variables [13,14]. This algorithm involves the calculation of the function to be maximized at vertices of certain simplexes in the parameter space but not the function's derivatives.

In our calculation we have used the following estimates of the maximum values of the spin-down parameters:

$$|\omega_k|_{\text{max}} = \frac{\omega_0}{(k+1) \tau_{\text{min}}^k}, \quad (6.10)$$

where τ_{min} is the minimum characteristic spin-down age of the neutron star. These estimates were adopted in the previous papers of this series and they were taken from the work of Brady *et al.* [1]. We have computed the fitting factor for three phase models with $s=0, 1, 2$, i.e., for a monochromatic signal, 1-spin-down signal, and 2-spin-down signal. We have carried out computations for two values of the spin-down age ($\tau_{\text{min}}=40$ y and $\tau_{\text{min}}=1000$ y), and for different values of the signal's frequency $f_0 = \omega_0 / (2\pi)$ and the observation time T_o . For each case we have made a calculation for a grid of positions of the source in the sky. We have chosen our observations to start from the beginning of the year 2000 (Julian day=2451545.0) and the position of the detector to coincide with the geographical location of the EXPLORER resonant bar.

Our results are summarized in Tables I, II, and III. For each grid of positions of the source in the sky we have found the minimum value FF_{min} of the fitting factor (the worst case). In the tables we have given the maximum length of the observation time for which FF_{min} is greater than 0.9, $0.9^{1/3}$, and 0.999. The conservative value of the fitting factor equal to $0.9^{1/3} \sim 0.967$ comes from the arguments of Apostolatos [10] by which such a fitting factor leads to an affordable 10%

TABLE I. Adequacy of the monochromatic linear model.

Frequency (Hz)	Maximal observation time T_o (h)					
	$\tau_{\min}=40$ years			$\tau_{\min}=1000$ years		
	$\text{FF}_{\min}>0.9$	$\text{FF}_{\min}>0.9^{1/3}$	$\text{FF}_{\min}>0.999$	$\text{FF}_{\min}>0.9$	$\text{FF}_{\min}>0.9^{1/3}$	$\text{FF}_{\min}>0.999$
100	4	3	2	8	7	4
200	3	3	1	6	6	3
300	3	2	1	6	5	3
400	2	2	1	5	5	3
500	2	2	1	5	4	3
600	2	2	1	5	4	2
700	2	2	1	5	4	2
800	2	2	1	4	4	2
900	2	2	1	4	4	2
1000	2	2	1	4	4	2

TABLE II. Adequacy of the 1-spin-down linear model.

Frequency (Hz)	Maximal observation time T_o (days)					
	$\tau_{\min}=40$ years			$\tau_{\min}=1000$ years		
	$\text{FF}_{\min}>0.9$	$\text{FF}_{\min}>0.9^{1/3}$	$\text{FF}_{\min}>0.999$	$\text{FF}_{\min}>0.9$	$\text{FF}_{\min}>0.9^{1/3}$	$\text{FF}_{\min}>0.999$
100	4	3	1	4	3	2
200	3	2	1	3	2	1
300	2	2	1	3	2	1
400	2	2	1	2	2	1
500	2	2	1	2	2	1
600	2	1	1	2	2	1
700	2	1	1	2	1	1
800	2	1	1	2	1	1
900	1	1	1	2	1	1
1000	1	1	1	2	1	1

TABLE III. Adequacy of the 2-spin-down linear model.

Frequency (Hz)	Maximal observation time T_o (days)					
	$\tau_{\min}=40$ years			$\tau_{\min}=1000$ years		
	$\text{FF}_{\min}>0.9$	$\text{FF}_{\min}>0.9^{1/3}$	$\text{FF}_{\min}>0.999$	$\text{FF}_{\min}>0.9$	$\text{FF}_{\min}>0.9^{1/3}$	$\text{FF}_{\min}>0.999$
100	14	12	8	14	12	8
200	13	11	7	13	11	7
300	11	9	6	12	10	6
400	10	9	5	10	9	5
500	9	8	5	9	8	5
600	9	8	5	9	8	5
700	9	7	5	9	7	5
800	8	7	4	8	7	4
900	8	7	4	8	7	4
1000	8	7	4	8	7	4

loss of events. The ultraconservative value of the fitting factor equal to 0.999 gives a negligible loss of 0.3% of events.

From the results presented in Tables I, II, and III it follows that the monochromatic linear model is adequate for a few hours of the observation time, the 1-spin-down model for a few days of the observation time, and the 2-spin-down model for around one week of the observation time. For several months of the observation time we do not expect to fit an adequate linear model; however, we know that for such long observation times a coherent all-sky search is computationally prohibitive [1,2]. Thus we conclude that in realistic (i.e., computationally feasible) coherent searches of not more than one week duration a satisfactory linear model can be chosen.

VII. SPACING OF FILTERS, THE SEARCH ALGORITHM, AND COMPUTATIONAL REQUIREMENTS

A. Grid of templates

In this section we shall present a construction of a grid in the parameter space on which the statistics \mathcal{F} will be calculated in order to search for signals. We assume that as a filter (or template), which we use in order to calculate the statistics, we shall use an approximation of the signal by a suitable linear model studied in Sec. VI. We would like to choose the grid in such a way that the additional loss of potential gravitational-wave signals due to the finite spacing of the grid is negligible. In order to determine an appropriate grid of templates we shall use the correlation function of the statistics \mathcal{F} . We shall choose the grid in such a way that the correlation function for two filters evaluated for parameters at two neighboring points of the grid is not less than a certain specified value.

This method is conceptually different from the approach that uses the Fisher matrix as a metric on the parameter space. However, when the Fisher matrix is constant, i.e., independent of the values of the parameters, which is the case for the linear model, the two approaches coincide. The metric approach is thus more general than ours as it does not require constancy of the parameter-space metric.

We consider here a constant amplitude signal

$$h(t; h_0, \Phi_0, \xi) = h_0 \sin[\Phi(t; \xi) + \Phi_0], \quad (7.1)$$

where Φ_0 is the initial phase of the wave form and the vector ξ collects all other phase parameters.

The correlation function C of the optimum statistics \mathcal{F} for signal (7.1) can be approximated using the Taylor expansion around $\tau=0$. Keeping terms at most quadratic in τ_i one gets

$$C(\tau) \approx 1 - \sum_{i,j} \tilde{\Gamma}_{ij} \tau_i \tau_j, \quad (7.2)$$

where the matrix $\tilde{\Gamma}$ has the components

$$\tilde{\Gamma}_{ij} := \left\langle \frac{\partial \Phi}{\partial \tau_i} \frac{\partial \Phi}{\partial \tau_j} \right\rangle - \left\langle \frac{\partial \Phi}{\partial \tau_i} \right\rangle \left\langle \frac{\partial \Phi}{\partial \tau_j} \right\rangle. \quad (7.3)$$

The matrix $\tilde{\Gamma}$ is the reduced Fisher information matrix for the signal (7.1) where the initial phase parameter Φ_0 has been reduced (see Sec. IV and Appendix B of Paper III for details).

The statistics \mathcal{F} can be expressed as a Fourier transform where the parameter p_0 corresponds to angular frequency and consequently \mathcal{F} can be calculated using the FFT algorithm. However, the FFT gives the values of the statistics on a certain grid of frequencies called Fourier frequencies. These frequencies in normalized units are separated by a factor of 2π . Thus when the true frequency falls between the two Fourier frequencies we cannot achieve the theoretical maximum of the optimal statistics \mathcal{F} . The worst case is when the frequency falls half way between the Fourier frequencies. One can easily find that in such a case the signal-to-noise ratio calculated approximately by means of the Taylor expansion of the correlation function is equal only to 0.42 of the optimal signal-to-noise ratio. This would lead to a drastic loss of signals. Therefore we need a finer grid. A way to achieve this and still take advantage of the speed of FFT, is to pad the time series with zeros.⁷ Padding with zeros of the length of the original time series gives a grid that is twice as fine as the Fourier grid, i.e., the difference between the Fourier frequencies is equal to π . Then in the worst case the signal-to-noise ratio is 0.89 of the optimal one. As we shall see later from Monte Carlo simulations this choice of spacing of the frequencies leads to a search algorithm where there is no additional loss of events due to bad grid spacing and the rms errors of the estimators of parameters are close to the theoretical minimum. It is also useful to note that the signal-to-noise ratio calculated from the exact correlation function formula yields the values of the fractions of the optimal signal-to-noise ratio equal to 0.63 and 0.90 for the difference between the Fourier frequencies equal to 2π and π , respectively. This indicates the limits of the validity of the Taylor expansion.

We introduce a convenient normalization of the spin-down parameters p_k of the linear model (6.1): namely,

$$\bar{p}_k := p_k T_o^{k+1}, \quad k=0, \dots, s. \quad (7.4)$$

This is equivalent to using a time coordinate $\bar{t} := t/T_o$ normalized by the total observation time T_o (then the normalized time duration of the signal is always 1). Using definition (7.4) the linear phase model (6.1), after dropping the initial phase parameter p , can be written as

⁷Padding time series with zeros of the length of the original time series in a real signal search means that we would need to calculate FFTs twice the length of the original data. This means doubling the computational time and the computer memory used. To avoid this pulsar astronomers have invented special interpolation algorithms that work in the Fourier domain and give twice as fine Fourier grid from the FFT of the original data. In the analysis of EXPLORER data we shall use one such algorithm provided to us by Duncan Lorimer (the details of which can be found in Ref. [15]).

$$\Phi(t; \xi) = \bar{p}_0 \frac{t}{T_o} + \sum_{k=1}^s \bar{p}_k \left(\frac{t}{T_o} \right)^{k+1} + A \cos(\Omega_r t) + B \sin(\Omega_r t), \quad (7.5)$$

where s is the number of spin downs included. In the quadratic approximation (7.2) and for the phase model (7.5), the equation

$$1 - \sum_{i,j} \tilde{\Gamma}_{ij} \tau_i \tau_j = C_0 = \text{const}, \quad (7.6)$$

describes the surface of the $(s+3)$ -dimensional correlation hyperellipsoid.

It is clear that we cannot fill the parameter space completely with hyperellipsoids. But such filling can be done by means of some prisms constructed with the aid of the correlation hyperellipsoid. We shall illustrate our construction in the special case of a 1-spin-down (i.e., $s=1$) linear phase model (7.5). In this case the components of the matrix $\tilde{\Gamma}$ as functions of the observation time are given by [here the order of the phase parameters is as follows: $\tau = (\Delta \bar{p}_0, \Delta \bar{p}_1, \Delta A, \Delta B)$]

$$\tilde{\Gamma} = \begin{pmatrix} 1/12 & 1/12 & 0 & -1/(2n\pi) \\ 1/12 & 4/45 & 1/(2n^2\pi^2) & -1/(2n\pi) \\ 0 & 1/(2n^2\pi^2) & 1/2 & 0 \\ -1/(2n\pi) & -1/(2n\pi) & 0 & 1/2 \end{pmatrix}, \quad (7.7)$$

where n is the observation time expressed in sidereal days, i.e., $n := (\Omega_r T_o) / (2\pi)$.

In the first step we choose spacing in the frequency parameter \bar{p}_0 to be equal to π . Then we compute the value C_0 of the correlation at the surface of the four-dimensional correlation hyperellipsoid (7.6) by requesting that the \bar{p}_0 axis intersects this surface at the points $\Delta \bar{p}_0 = \pm \pi/2$. Substituting $\tau = (\Delta \bar{p}_0, 0, 0, 0)$ into Eq. (7.6), one gets

$$C_0 = 1 - \tilde{\Gamma}_{\bar{p}_0 \bar{p}_0} \Delta \bar{p}_0^2 = 1 - \frac{\pi^2}{48} \approx 0.79. \quad (7.8)$$

Making use of Eqs. (7.7) and (7.8), the general equation (7.6) can be written in the case of the 1-spin-down signal in the form [we also substitute $\tau = (\bar{p}_0, \bar{p}_1, A, B)$]

$$A^2 + B^2 + \frac{1}{6} \bar{p}_0^2 + \frac{1}{3} \bar{p}_0 \bar{p}_1 + \frac{8}{45} \bar{p}_1^2 + 2\zeta^2 A \bar{p}_1 - 2\zeta B(\bar{p}_0 + \bar{p}_1) - \frac{\pi^2}{24} = 0, \quad (7.9)$$

where we have introduced

$$\zeta := \frac{1}{n\pi}. \quad (7.10)$$

We first construct the elementary cell of the grid in the *filter space* (which is the space spanned by the parameters

\bar{p}_1 , A , and B). We consider the $\bar{p}_0=0$ cross section of the four-dimensional hyperellipsoid (7.9). This cross section defines the three-dimensional ellipsoid in the (\bar{p}_1, A, B) space:

$$(A + \zeta^2 \bar{p}_1)^2 + (B - \zeta \bar{p}_1)^2 = \frac{\pi^2}{24} - \left(\frac{8}{45} - \zeta^2 - \zeta^4 \right) \bar{p}_1^2 \quad (7.11)$$

(let us note that $8/45 - \zeta^2 - \zeta^4 > 0$ for $n \geq 1$). Next we take the cross sections of the ellipsoid (7.11) with the planes $\bar{p}_1 = \pm \delta$ for some positive constant δ . These cross sections define two adjacent circles. We inscribe two regular hexagons into these circles. The hexagons form the bases of the inclined prism inscribed in the ellipsoid (7.11). The three-dimensional volume of this prism reads

$$V(\delta) = 3\sqrt{3} \left[\frac{\pi^2}{24} - \left(\frac{8}{45} - \zeta^2 - \zeta^4 \right) \delta^2 \right] \delta. \quad (7.12)$$

Then we maximize the volume $V(\delta)$ with respect to δ . The function $V(\delta)$ attains its maximal value for

$$\delta_{\max} = \frac{\pi}{6\sqrt{2} \sqrt{\frac{8}{45} - \zeta^2 - \zeta^4}}. \quad (7.13)$$

The maximal value $V(\delta_{\max})$ of the volume (7.12) is the volume of the elementary cell in the filter space. It reads

$$V_{\text{gr}} = \frac{\pi^3}{24\sqrt{6} \sqrt{\frac{8}{45} - \zeta^2 - \zeta^4}}. \quad (7.14)$$

Equation (7.14) gives the following values of the volume V_{gr} of the elementary cell in the filter space: $V_{\text{gr}} = 2.05, 1.35, 1.29, 1.27$ for $n = 1, 2, 3, 4$, respectively.

We construct the elementary cell in the four-dimensional space $(\bar{p}_0, \bar{p}_1, A, B)$ as follows. We parallelly translate in four dimensions and in two opposite directions the three-dimensional prism of maximal volume, which is described above and that lies in the $\bar{p}_0=0$ subspace, into the subspaces $\bar{p}_0 = -\pi/2$ and $\bar{p}_0 = +\pi/2$. We choose one of the principal directions⁸ of the hyperellipsoid (7.9) as the direction of translation. Such a constructed elementary cell is the four-dimensional prism whose bases are two adjacent three-dimensional hexagonal prisms lying in the $\bar{p}_0 = -\pi/2$ and $\bar{p}_0 = +\pi/2$ subspaces.

It is clear from the construction that our elementary cell will stick out the four-dimensional hyperellipsoid (7.9). For the case of $n=2$ we have calculated the correlation function $C(\tau) = 1 - \sum_{i,j} \tilde{\Gamma}_{ij} \tau_i \tau_j$ at all vertices of the elementary cell and we have found that the smallest value of $C(\tau)$ is equal to 0.77. Thus the grid constructed above ensures that the corre-

⁸The reasonable result one obtains only when translating along this principal direction of the hyperellipsoid (7.9), which almost coincides with the \bar{p}_0 axis.

lation between the filter and the signal is not less than 0.77. The Monte Carlo simulations presented below show that by using such a grid we do not lose any signals and that rms errors of the parameter estimators are very close to the minimum ones allowed by the Cram r-Rao bound.

If as a base of the elementary cell in the filter space we choose a square instead of a regular hexagon the volume of the cell (independently of the value of n) decreases by a factor of $3\sqrt{3}/4 \sim 1.3$.

B. Monte Carlo simulations

In order to test the effectiveness of the chosen grid we have made Monte Carlo simulations of the detection of our signal in the noise and estimation of its parameters. In the simulations we have taken the signal s to be a 1-spin-down linear model with a constant amplitude h_0 :

$$s(t) = h_0 \exp \left\{ i \left[p + p_0 t + p_1 t^2 + A \cos \left(\frac{2\pi n t}{T_o} \right) + B \sin \left(\frac{2\pi n t}{T_o} \right) \right] \right\}, \quad (7.15)$$

where T_o is the observation time and n is the integer equal to the number of sidereal days of observation in real search. The simulation of the parameter estimation of the accurate signal with the phase given by Eq. (6.3) is presented in Sec. VII C. In the case of signal (7.15) the maximum likelihood detection involves finding the global maximum of the functional \mathcal{F}_s with respect to the parameters p_0 , p_1 , A , B . The functional \mathcal{F}_s is given by

$$\mathcal{F}_s = \frac{2|\tilde{X}|^2}{S_h T_o}, \quad (7.16)$$

where

$$\tilde{X} = \int_0^{T_o} x(t) \exp \left\{ -i \left[p_1 t^2 + A \cos \left(\frac{2\pi n t}{T_o} \right) + B \sin \left(\frac{2\pi n t}{T_o} \right) \right] \right\} \exp(-ip_0 t) dt. \quad (7.17)$$

In Eq. (7.17) the data $x(t) = s(t) + n(t)$, where $n(t)$ is the stationary noise with spectral density S_h . In our simulations we have generated white and Gaussian noise $n(t)$. Thus our statistics \mathcal{F}_s consists of taking the modulus of the Fourier transform of the data demodulated for a grid of parameters p_1 , A , and B . To find the maximum of \mathcal{F}_s we have used a hierarchical algorithm consisting of two steps: a *coarse* search and a *fine* search. The coarse search involves the calculation of \mathcal{F}_s on the grid in the parameter space constructed in Sec. VII A and finding the maximum value of \mathcal{F}_s on that grid. The values of the parameters of the filter that give the maximum are coarse estimates of the parameters of the signal. The fine search involves finding the maximum of \mathcal{F}_s using a maximization routine with the starting values of the parameters equal to the coarse estimates of the parameters. As a maximization routine we have used the Nelder-Mead

simplex algorithm. We plan to use the above hierarchical procedure in the analysis of real data from the EXPLORER detector.

The procedure described above differs from another two-step hierarchical algorithm proposed by Mohanty and Dhurandhar [8,9]. The first step of the two procedures is the same but in the second step Mohanty and Dhurandhar propose to use a fine grid in the parameter space around the maximum obtained from the coarse search whereas we propose to use a maximization routine. However, as any optimization routine the Nelder-Mead algorithm may fail to find the global maximum. Therefore in the real data search we may have to use a combination of both hierarchical procedures: whenever our maximization routine fails we use a fine search proposed by Mohanty and Dhurandhar as the second step.

We have performed Monte Carlo simulations by generating a signal $s(t)$ given by Eq. (7.15) and adding white Gaussian noise $n(t)$. By adjusting the amplitude h_0 we have generated a signal with a chosen optimal signal-to-noise ratio d . In our simulations we have chosen the observation time to be $n = 2$. We have done 1000 runs for several values of d . We have compared the standard deviations of the parameter estimators obtained from the simulations with the theoretical ones calculated from the Cram r-Rao bound. We have also compared the probability of detection of the signal obtained from the simulations with the theoretical one calculated from Eq. (3.8). In our simulations we have used the hexagonal grid constructed in Sec. VII A.

The results of our computations are depicted in Fig. 1. We have observed that above a certain signal-to-noise ratio (that we shall call the *threshold signal-to-noise ratio*) the results of the Monte Carlo simulations agree very well with the calculations of the rms errors from the covariance matrix. However, below the threshold signal-to-noise ratio they differ by a large factor. This threshold effect is well known in signal processing [16] and has also been observed in numerical simulations for the case of a coalescing binary chirp signal [17,18]. As was explained in Sec. VII of Paper III this effect arises because sometimes the global maximum of the functional \mathcal{F}_s occurs as a result of noise and not the signal. This happens the more often the lower the signal-to-noise ratio. Following the theory of this effect developed in Paper III we have calculated the approximate rms errors of the estimators of the parameters. They are shown as thick lines in Fig. 1.

The comparison of the probability of detection obtained from the simulations with the theoretical formula (3.8) shows that for lower signal-to-noise ratios we have more detections than expected. This is because the theoretical formula assumes that when the signal is detected its parameters are located in the cell corresponding to the true parameters of the signal. However, in practice for lower values of d as a result of the noise the signal may drift to neighboring cells. Thus for a threshold signal-to-noise ratio of 7 we find that the simulated probability of detection is 5% greater than the theoretical one whereas for signal-to-noise 8 and greater the simulated and the theoretical probabilities of detection agree within 0.5%.

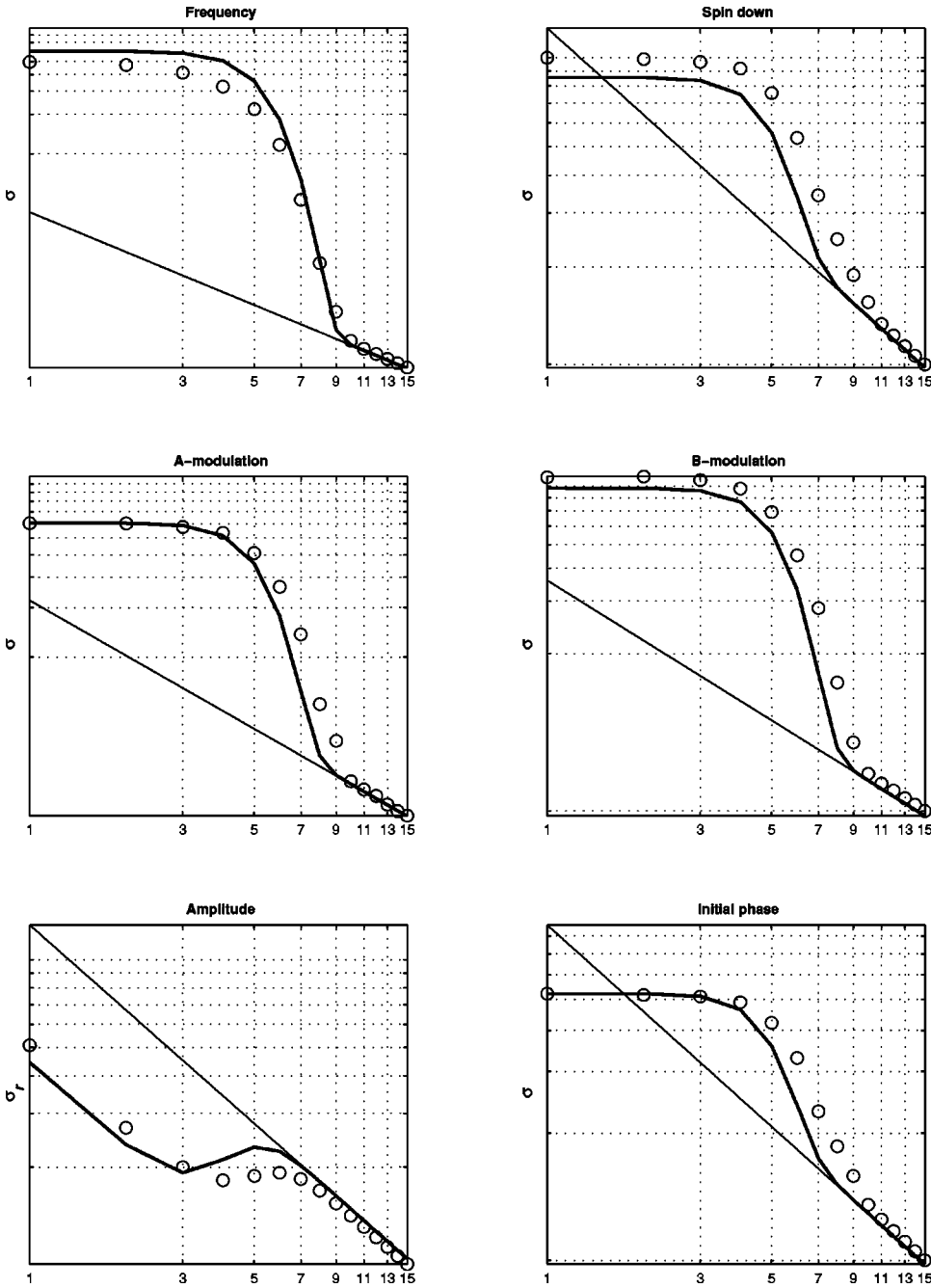


FIG. 1. Monte Carlo simulations of the rms errors of the parameter estimators of the signal given by Eq. (7.15) for $n=2$. The x axes are labeled by the optimal signal-to-noise ratio d . The y axes are labeled by the standard deviation σ except for the case of the amplitude parameter where the relative rms error $\sigma_r := \sigma/h_0$ is given. Both σ and σ_r are dimensionless. The results of simulations of 1000 runs for each value of d are marked by the circles. The thin solid lines are calculated from the covariance matrix and they constitute the Cramér-Rao bound, i.e., the smallest rms error for an unbiased estimator. The thick solid lines are calculated from a model that takes into account the false alarms.

C. Estimation of parameters of the signal

Once the optimal statistics, calculated with the linear filter of Sec. VI, crosses a chosen threshold we register the estimates of the parameters p_0 , p_1 , A , and B . We would like to estimate physically interesting parameters: frequency, spin down, declination, and right ascension of the source. We propose the following algorithm to achieve this. From Eqs. (7.18) and the least-squares fit of the linear model to the accurate model of the signal we calculate the approximate values of parameters ω_0 , ω_1 , δ , α . Then using the accurate model of the signal as a filter we search for accurate estimates of the parameters on a small grid around the approximate estimates.

We have made Monte Carlo simulations of the above procedure by making 100 runs for one position of the source in

the sky and for five signal-to-noise ratios: 8, 12, 16, 20, 24. First of all we have found that the probability of detection of the signal from simulation agrees within 0.5% with the theoretical one. Concerning the accuracy of the parameter estimation we have obtained that rms errors for declination and right ascension were very close to their Cramér-Rao bounds; however, the rms errors for frequency and spin down were worse. The mean biases in the estimators of the parameters ω_0 , ω_1 , δ , and α were less than 0.1%, 0.5%, 0.005%, and 0.01%, respectively.

D. Amplitude modulation

Approximation of the continuous gravitational-wave signal by a simple linear model and consequently the approxi-

mation of the optimal statistics \mathcal{F} , Eq. (3.3), by a homogeneous random field were studied under the assumption that the amplitude of the signal was constant. However, as the modulation of the amplitude of the signal is very slow (it changes on a time scale of one sidereal day) in comparison to the rapid modulation of the phase we expect that our linear model of the phase is a satisfactory approximation of the phase of the optimal filters given by Eqs. (3.4). We also expect that the calculation of the number of elementary cells (except for a factor of 2, see below) and construction of the grid in the parameter space given in Sec. VII A above are valid for the amplitude-modulated signal.

To calculate the optimal statistics \mathcal{F} , we first need to correct the time series for amplitude modulation, i.e., multiply the time series by the functions $a(t)$ and $b(t)$. Our grid is on the space parametrized by p_0 , p_1 , A , and B whereas the functions $a(t)$ and $b(t)$ depend on the declination δ and the right ascension α . From Eqs. (6.2) we have the following expressions for δ and α in terms of A and B :

$$\delta = \pm \arccos\left(\frac{\sqrt{A^2 + B^2}}{\frac{\omega_0 r}{c}}\right), \quad (7.18a)$$

$$\alpha = \phi_r + \arctan\left(\frac{B}{A}\right). \quad (7.18b)$$

Since for each set of parameters A and B there are two sets of parameters δ and α the number of cells needs to be multiplied by a factor of 2 and this number is to be used to compute from Eq. (3.5) the threshold corresponding to a given false alarm probability.

We see that the declination δ of the source, Eq. (7.18a), depends on the angular frequency ω_0 of the signal that we do not know before we detected the signal. The uncertainty in δ affects the constant amplitudes in front of the time-dependent modulation factors. However, for the case of the EXPLORER detector data (which we plan to analyze employing the methods developed above) we have that frequency f_0 is around 1 kHz within the band $B \sim 1$ Hz (see Sec. VIII). Thus by choosing in the equation for declination δ the frequency equal to the middle frequency of the band to be analyzed instead of the unknown frequency ω_0 , we shall lose at most only a fraction $\sim B/(2f_0) \sim 0.0005$ of the signal-to-noise ratio.

E. Computational requirements

To estimate the computational requirements to do the search we calculate the number of FFTs that one needs to compute. This number depends on the total volume V_F of the filter space, which is given by

$$V_F = \int \int_{B_2(0, r_o)} dA \, dB \int_{-\omega_{\max} T_o^2/(2\tau_{\min})}^{\omega_{\max} T_o^2/(2\tau_{\min})} d\bar{p}_1, \quad (7.19)$$

where ω_{\max} is the maximum angular frequency of the signal and $B_2(0, r_o)$ is a two-dimensional disc in the (A, B) plane of radius r_o ,

$$r_o = \frac{\omega_{\max} r}{c}. \quad (7.20)$$

Thus we get

$$V_F = \frac{\pi}{c^2} \frac{\omega_{\max}^3 r^2 T_o^2}{\tau_{\min}}. \quad (7.21)$$

The number of grid points on which the optimal statistics \mathcal{F} , Eq. (3.3), should be calculated is obtained by dividing the volume V_F of the filter space by the volume V_{gr} of the elementary cell of the chosen grid in the filter space. In Sec. VII D we have found that for each set of parameters A and B there are two sets of parameters δ and α [see Eqs. (7.18)]. Moreover, the optimal statistics involves calculations of two FFTs — F_a and F_b [see Eqs. (3.3) and (3.4)]. Thus the total number N_{FFT} of FFTs is four times the number of grid points and it is given by

$$N_{\text{FFT}} = 4 \frac{V_F}{V_{\text{gr}}}. \quad (7.22)$$

Assuming that the data processing rate should be comparable to the data acquisition rate and that the data processing consists only of computing the FFTs the number \mathcal{P} of floating point operations per second (flops) can be estimated by

$$\mathcal{P} = 6 \Delta \nu N_{\text{FFT}} [\log_2(2 \Delta \nu T_o) + \frac{1}{2}], \quad (7.23)$$

where $\Delta \nu = (\omega_{\max} - \omega_s)/(2\pi)$ is the bandwidth of the search. Equation (7.23) does not take into account the computational requirements to do the fine search. This is because the fine search will only be triggered when there is threshold crossing and this as estimated in the next section will be a rare event. It is worth pointing out that the formula (7.23) coincides with the analogous formula for a broadband search (see, e.g., Ref. [1]) with the maximum frequency replaced by the bandwidth of the search.

VIII. A NARROW-BAND ALL-SKY SEARCH OF EXPLORER DATA

The data analysis tools for searching continuous gravitational-wave signals that we have developed in the preceding sections of the present work can be applied both to the resonant bar and the laser interferometric detectors. We plan to apply these tools to the data from the resonant bar detector EXPLORER⁹ [19]. The detector has already collected many years of data with a high duty cycle (e.g., in 1991 the duty cycle was 75%). Our primary objective is to carry out an all-sky search. It is a unique property of the gravitational-wave detectors that with a single time series one can search for signals coming from all sky directions. In the case of other instruments like optical and radio telescopes to cover the whole or even part of the sky requires a large

⁹The EXPLORER detector is operated by the ROG Collaboration located in Italian Istituto Nazionale di Fisica Nucleare (INFN); see <http://www.roma1.infn.it/rog/explorer/explorer.html>.

amount of expensive telescope time. The directed search of the galactic center has already been carried out and limits for the amplitude of the gravitational waves has been established [20].

The EXPLORER detector is most sensitive over certain two narrow bandwidths (called minus and plus modes) of about 1 Hz wide at two frequencies around 1 kHz. To make the search computationally feasible we propose an all-sky search of data of a few days long in the narrow band where the detector has the best sensitivity. By narrowing the bandwidth of the search we can shorten the length of the data to be analyzed as we need to sample the data at only twice the bandwidth and thus we reduce the computational time. To reduce the parameter space to search we restrict ourselves to only one spin-down parameter. We would also like to use the linear filter model as the search template. Then as our frequency is around 1 kHz from Table II we read that we can consider up to 2 days of coherent observation time in order that the fitting factor is greater than 0.9. For the sake of the FFT algorithm it is best to keep the length of the data to be a power of 2. Consequently we choose the number of data points to analyze to be $N=2^{18}$. Then for $T_o=2$ days of observation time the bandwidth $\Delta\nu$ of the data will be $\Delta\nu = N/(2T_o) \sim 0.76$ Hz. We also choose to analyze the data for the plus mode which has frequency around 922 Hz. With these parameters we can calculate the number of filters that we need to compute. From Eq. (7.22) and for the hexagonal grid over the sky we get that $N_{\text{FFT}} \sim 3.7 \times 10^8$. Assuming that the data processing rate should be comparable to the data acquisition rate the computing power required [calculated by means of Eq. (7.23)] is around 7.7 Gflops. If we allow a month for off-line processing of data with the above parameters we only need around 250 Mflops of computer power.

From Eq. (3.11) we can calculate the threshold that we need to set. For example, choosing the false alarm probability to be 1% we find by inverting Eq. (3.11) and using Eq. (3.10) that for the parameters that we have chosen above the threshold signal-to-noise ratio is 8.3. However, we know that in the coarse search we are using a suboptimal filter and we are losing the signal-to-noise ratio. For the parameters of our search we find that in the worst case the fitting factor is 0.94. Moreover, due to our discrete grid in the parameter space the signal-to-noise ratio can decrease in the worst case by an additional factor of $\sqrt{0.77} \sim 0.88$. Thus in the worst case the signal-to-noise ratio of our coarse search can be a factor of 0.83 of the optimal one. Hence in order not to lose any signals we lower the signal-to-noise threshold by a factor of 0.83. By lowering the threshold we must make sure that the number of false alarms does not increase excessively. From Eq. (3.12) we find that the expected number of false alarms with the lower threshold is ~ 310 . This is certainly a manageable number that will insignificantly increase the computational time of the total search. We can consider lowering the threshold even further in order to have more candidate events that can be later verified using longer stretches of data. For example, by lowering the threshold by a factor of 0.8 the expected number of false alarms is around 1600 which will still be manageable to verify.

The minimum detectable amplitude h_0 , i.e., the amplitude

for which the signal-to-noise ratio is equal to 1, is given by

$$h_0 = \sqrt{\frac{S_h}{T_o}}, \quad (8.1)$$

where S_h is the *one-sided* spectral density of noise. For two days of observation time T_o and spectral density S_h at the plus mode equal to 2×10^{-42} /Hz, the minimum detectable amplitude is 3.4×10^{-24} . In order that we have a detection with 99% confidence by the calculation above we need a signal-to-noise ratio of 8.3 and thus the amplitude of the signal must be around 2.8×10^{-23} . Consequently by the estimate given in Eq. (2.3) a continuous gravitational-wave signal from a neutron star located at a distance of 1 kpc, spinning with period of 2 ms, and with ellipticity $\epsilon \sim 10^{-5}$ will be detectable.

ACKNOWLEDGMENTS

One of us (A.K.) would like to thank the ROG group in Istituto Nazionale di Fisica Nucleare (INFN), Frascati, Italy, where part of this work was done, for hospitality and Consiglio Nazionale delle Ricerche (CNR) for support within the exchange agreement with the Polish Academy of Sciences. This work was supported in part by the KBN Grant No. 2 P03B 094 17 (K.M.B., P.J., and A.K.). We would also like to thank the Interdisciplinary Center for Mathematical and Computational Modeling of Warsaw University for computing time.

APPENDIX A: BEAM-PATTERN FUNCTIONS

1. Interferometric beam-pattern functions

Noise-free response function h of the laser interferometric detector is defined as the difference between the wave-induced relative length changes of the two interferometer arms. The derivation of formula (2.1) in the case of the laser interferometer can be found, e.g., in Sec. II A of Ref. [20].

Explicit formulas for the interferometric beam-pattern functions F_+ and F_\times from Eq. (2.1) are derived, e.g., in Sec. II A of Ref. [2]. The functions read

$$F_+(t) = \sin \zeta [a(t) \cos 2\psi + b(t) \sin 2\psi], \quad (\text{A1a})$$

$$F_\times(t) = \sin \zeta [b(t) \cos 2\psi - a(t) \sin 2\psi], \quad (\text{A1b})$$

where

$$\begin{aligned} a(t) = & \frac{1}{4} \sin 2\gamma (1 + \sin^2 \phi) (1 + \sin^2 \delta) \cos[2(\alpha - \phi_r - \Omega_r t)] \\ & - \frac{1}{2} \cos 2\gamma \sin \phi (1 + \sin^2 \delta) \sin[2(\alpha - \phi_r - \Omega_r t)] \\ & + \frac{1}{4} \sin 2\gamma \sin 2\phi \sin 2\delta \cos(\alpha - \phi_r - \Omega_r t) \\ & - \frac{1}{2} \cos 2\gamma \cos \phi \sin 2\delta \sin(\alpha - \phi_r - \Omega_r t) \\ & + \frac{3}{4} \sin 2\gamma \cos^2 \phi \cos^2 \delta, \end{aligned} \quad (\text{A2a})$$

$$\begin{aligned}
b(t) = & \cos 2\gamma \sin \phi \sin \delta \cos[2(\alpha - \phi_r - \Omega_r t)] \\
& + \frac{1}{2} \sin 2\gamma (1 + \sin^2 \phi) \sin \delta \sin[2(\alpha - \phi_r - \Omega_r t)] \\
& + \cos 2\gamma \cos \phi \cos \delta \cos(\alpha - \phi_r - \Omega_r t) \\
& + \frac{1}{2} \sin 2\gamma \sin 2\phi \cos \delta \sin(\alpha - \phi_r - \Omega_r t). \quad (\text{A2b})
\end{aligned}$$

In Eqs. (A1) ζ is the angle between the interferometer arms (usually $\zeta=90^\circ$) and ψ is the polarization angle of the wave. In Eqs. (A2) the angles α and δ are, respectively, the right ascension and declination of the gravitational-wave source. The geodetic latitude of the detector's site is denoted by ϕ [its precise definition is given in Eq. (5.1a)], the angle γ determines the orientation of the detector's arms with respect to local geographical directions: γ is measured counterclockwise from the east to the bisector of the interferometer arms. The rotational angular velocity of Earth is denoted by Ω_r , and ϕ_r is a deterministic phase which defines the position of Earth in its diurnal motion at $t=0$ (the sum $\phi_r + \Omega_r t$ essentially coincides with the local sidereal time of the detector's site, i.e., with the angle between the local meridian and the vernal point; see Sec. V B).

2. Bar beam-pattern functions

We consider here the response of a bar detector to a weak plane gravitational wave in the long wavelength approximation. Moreover, we assume that the frequency spectrum of the gravitational wave which hits the bar entirely lies within the sensitivity band of the detector. Under these assumptions the dimensionless response function h of the bar detector can be computed from the formula (cf. Sec. 9.5.2 in Ref. [21])

$$h(t) = \mathbf{n} \cdot [\tilde{H}(t)\mathbf{n}], \quad (\text{A3})$$

where \mathbf{n} denotes the unit vector parallel to the symmetry axis of the bar, \tilde{H} is the three-dimensional matrix of the spatial metric perturbation produced by the wave in the proper reference frame of the detector, and a dot stands for the standard scalar product in the three-dimensional Cartesian space. In the detector's reference frame we introduce Cartesian coordinates (x_d, y_d, z_d) with the z_d axis along Earth's radius pointing toward the zenith, and the x_d axis along the bar's axis of symmetry. In these coordinates the vector \mathbf{n} from Eq. (A3) has components

$$\mathbf{n} = (1, 0, 0). \quad (\text{A4})$$

In the wave Cartesian coordinate system (x_w, y_w, z_w) (in which the wave travels in the $+z_w$ direction), the three-dimensional matrix H of the wave-induced spatial metric perturbation has components

$$H(t) = \begin{pmatrix} h_+(t) & h_\times(t) & 0 \\ h_\times(t) & -h_+(t) & 0 \\ 0 & 0 & 0 \end{pmatrix}, \quad (\text{A5})$$

where the functions h_+ and h_\times describe two independent wave's polarizations. The matrices \tilde{H} and H are related through the equation

$$\tilde{H}(t) = M(t)H(t)M(t)^T, \quad (\text{A6})$$

where M is the three-dimensional orthogonal matrix of transformation from the wave coordinates to the detector coordinates, T denotes the matrix transposition. Collecting Eqs. (A3)–(A6) together one can see that the response function h is a linear combination of the functions h_+ and h_\times :

$$h(t) = F_+(t)h_+(t) + F_\times(t)h_\times(t), \quad (\text{A7})$$

where F_+ and F_\times are beam-pattern functions.

Because of the diurnal motion of the Earth the beam-patterns F_+ and F_\times are periodic functions of time with a period equal to one sidereal day. We want to express F_+ and F_\times as functions of the right ascension α and the declination δ of the gravitational-wave source and the polarization angle ψ (the angles α , δ , and ψ determine the orientation of the wave reference frame with respect to the celestial reference frame defined below). We represent the matrix M of Eq. (A6) as

$$M = M_3 M_2 M_1^T \quad (\text{A8})$$

where M_1 is the matrix of transformation from wave to celestial frame coordinates, M_2 is the matrix of transformation from celestial coordinates to cardinal coordinates, and M_3 is the matrix of transformation from cardinal coordinates to detector coordinates. In celestial coordinates the z axis coincides with the Earth's rotation axis and points toward the North pole, the x and y axes lie in the Earth's equatorial plane, and the x axis points toward the vernal point. In cardinal coordinates the (x, y) plane is tangent to the surface of the Earth at the detector's location with the x axis in the north-south direction and the y axis in the west-east direction, the z cardinal axis is along Earth's radius pointing toward the zenith. Under the above conventions the matrices M_1 , M_2 , and M_3 are as follows (matrices M_1 and M_2 are taken from Sec. II A of Ref. [2])

$$M_1 = \begin{pmatrix} \sin \alpha \cos \psi - \cos \alpha \sin \delta \sin \psi & -\cos \alpha \cos \psi - \sin \alpha \sin \delta \sin \psi & \cos \delta \sin \psi \\ -\sin \alpha \sin \psi - \cos \alpha \sin \delta \cos \psi & \cos \alpha \sin \psi - \sin \alpha \sin \delta \cos \psi & \cos \delta \cos \psi \\ -\cos \alpha \cos \delta & -\sin \alpha \cos \delta & -\sin \delta \end{pmatrix}, \quad (\text{A9a})$$

$$M_2 = \begin{pmatrix} \sin \phi \cos(\phi_r + \Omega_r t) & \sin \phi \sin(\phi_r + \Omega_r t) & -\cos \phi \\ -\sin(\phi_r + \Omega_r t) & \cos(\phi_r + \Omega_r t) & 0 \\ \cos \phi \cos(\phi_r + \Omega_r t) & \cos \phi \sin(\phi_r + \Omega_r t) & \sin \phi \end{pmatrix}, \quad (\text{A9b})$$

$$M_3 = \begin{pmatrix} -\sin \gamma & \cos \gamma & 0 \\ -\cos \gamma & -\sin \gamma & 0 \\ 0 & 0 & 1 \end{pmatrix}. \quad (\text{A9c})$$

In Eq. (A9b) ϕ is the geodetic latitude of the detector's site, Ω_r is the rotational angular velocity of Earth, and the phase ϕ_r defines the position of Earth in its diurnal motion at $t = 0$ (the sum $\phi_r + \Omega_r t$ essentially coincides with the local sidereal time of the detector's site; see Sec. VB in the present paper). In Eq. (A9c) γ determines the orientation of the bar's axis of symmetry with respect to local geographical directions, it is measured counterclockwise from the east to the bar's axis of symmetry.

To find the explicit formula for F_+ and F_\times we have to combine Eqs. (A3)–(A9). After some algebraic manipulations we arrive at the expressions:

$$F_+(t) = a(t) \cos 2\psi + b(t) \sin 2\psi, \quad (\text{A10a})$$

$$F_\times(t) = b(t) \cos 2\psi - a(t) \sin 2\psi, \quad (\text{A10b})$$

where

$$\begin{aligned} a(t) = & \frac{1}{2}(\cos^2 \gamma - \sin^2 \gamma \sin^2 \phi)(1 + \sin^2 \delta) \cos[2(\alpha - \phi_r \\ & - \Omega_r t)] + \frac{1}{2} \sin 2\gamma \sin \phi (1 + \sin^2 \delta) \sin[2(\alpha - \phi_r \\ & - \Omega_r t)] - \frac{1}{2} \sin^2 \gamma \sin 2\phi \sin 2\delta \cos[\alpha - \phi_r - \Omega_r t] \\ & + \frac{1}{2} \sin 2\gamma \cos \phi \sin 2\delta \sin(\alpha - \phi_r - \Omega_r t) \\ & + \frac{1}{2}(1 - 3 \sin^2 \gamma \cos^2 \phi) \cos^2 \delta, \end{aligned} \quad (\text{A11a})$$

$$\begin{aligned} b(t) = & -\sin 2\gamma \sin \phi \sin \delta \cos[2(\alpha - \phi_r - \Omega_r t)] + (\cos^2 \gamma \\ & - \sin^2 \gamma \sin^2 \phi) \sin \delta \sin[2(\alpha - \phi_r - \Omega_r t)] \\ & - \sin 2\gamma \cos \phi \cos \delta \cos(\alpha - \phi_r - \Omega_r t) \\ & - \sin^2 \gamma \sin 2\phi \cos \delta \sin(\alpha - \phi_r - \Omega_r t). \end{aligned} \quad (\text{A11b})$$

In Eqs. (A10) and (A11) α , δ , ψ , ϕ , Ω_r , and ϕ_r all have the same meaning as in Eqs. (A1)–(A2); the angle γ determines the orientation of the bar detector with respect to local geographical directions: γ is measured counterclockwise from the east to the bar's axis of symmetry.

Equivalent explicit formulas for the functions a and b from Eqs. (A11) can be found in Ref. [22] where different angles describing the position of the gravitational-wave

source in the sky and the orientation of the detector on Earth are used.¹⁰

APPENDIX B: THE TIME AVERAGES $\langle a^2 \rangle$ AND $\langle b^2 \rangle$

1. Laser interferometric detector

The time averages $\langle a^2 \rangle$ and $\langle b^2 \rangle$ entering Eqs. (3.1), for the observation time T_o chosen as an integer number of sidereal days, for the laser interferometric detector take the form (here n is a positive integer):

$$\begin{aligned} \langle a^2 \rangle|_{T_o = n2\pi/\Omega_r} = & \frac{1}{16} \sin^2 2\gamma [9 \cos^4 \phi \cos^4 \delta + \frac{1}{2} \sin^2 2\phi \\ & \times \sin^2 2\delta + \frac{1}{32} (3 - \cos 2\phi)^2 (3 - \cos 2\delta)^2] \\ & + \frac{1}{32} \cos^2 2\gamma [4 \cos^2 \phi \sin^2 2\delta \\ & + \sin^2 \phi (3 - \cos 2\delta)^2], \end{aligned} \quad (\text{B1a})$$

$$\begin{aligned} \langle b^2 \rangle|_{T_o = n2\pi/\Omega_r} = & \frac{1}{32} \sin^2 2\gamma [(3 - \cos 2\phi)^2 \sin^2 \delta \\ & + 4 \sin^2 2\phi \cos^2 \delta] + \frac{1}{4} \cos^2 2\gamma \\ & \times (1 + \cos 2\phi \cos 2\delta). \end{aligned} \quad (\text{B1b})$$

We see that $\langle a^2 \rangle$ and $\langle b^2 \rangle$ depend only on one unknown parameter of the signal—the declination δ of the gravitational-wave source. They also depend on the latitude ϕ of the detector's location and the orientation γ of the detector's arms with respect to local geographical directions.

2. Resonant bar detector

For the resonant bar detector the time averages $\langle a^2 \rangle$ and $\langle b^2 \rangle$, for the observation time T_o being an integer number of sidereal days, have the form

$$\begin{aligned} \langle a^2 \rangle|_{T_o = n2\pi/\Omega_r} = & \frac{1}{4} (1 - 3 \sin^2 \gamma \cos^2 \phi)^2 \cos^4 \delta \\ & + \frac{1}{2} \sin^2 \gamma \cos^2 \phi (1 - \sin^2 \gamma \cos^2 \phi) \sin^2 2\delta \\ & + \frac{1}{8} [\sin^2 2\gamma \sin^2 \phi + (\cos^2 \gamma \\ & - \sin^2 \gamma \sin^2 \phi)^2] (1 + \sin^2 \delta)^2, \end{aligned} \quad (\text{B2a})$$

¹⁰Our functions a and b from Eqs. (A11) are identical with the functions \mathcal{S}_+ and \mathcal{S}_\times from Eqs. (2.90) and (2.91) of Ref. [22], provided the following identification of the variables η , α , θ , Ψ used in [22] with our variables Ω_r , ϕ_r , α , δ , ϕ , γ is made: $\eta \rightarrow -(\alpha - \phi_r - \Omega_r t)$, $\alpha \rightarrow \pi/2 - \delta$, $\theta \rightarrow \pi/2 - \phi$, $\Psi \rightarrow \gamma - \pi/2$.

$$\begin{aligned} \langle b^2 \rangle|_{T_o=n2\pi/\Omega_r} = & \frac{1}{2}(\sin^2 2\gamma \cos^2 \phi + \sin^4 \gamma \sin^2 2\phi) \cos^2 \delta \\ & + \frac{1}{2}(\cos^4 \gamma + \frac{1}{2} \sin^2 2\gamma \sin^2 \phi \\ & + \sin^4 \gamma \sin^4 \phi) \sin^2 \delta. \end{aligned} \quad (\text{B2b})$$

As in the case of the laser interferometric detector, the time averages $\langle a^2 \rangle$ and $\langle b^2 \rangle$ depend on the declination δ of the gravitational-wave source, the latitude ϕ of the detector's location, and the orientation γ of the detector's axis of symmetry with respect to local geographical directions.

APPENDIX C: THE TOP2BARY PROCEDURE

The algorithms described in Sec. V were implemented in an easily callable subroutine named TOP2BARY consisting of about 900 lines of FORTRAN code. The ephemeris files (DE405'90.'10, tai-utc.dat, and yearly eopc04.yy) required by the program must be kept in the directory \Top2Bary\EphData on the current disk. The procedure header is shown below.

```
subroutine Top2Bary (CJD_E, clat, clong, height, pve, pvo)
c Procedure to calculate position (km) and velocity (km/s) of an observatory
c located at given geographical position (conventional coordinates in degrees
c and height above the Earth ellipsoid in m) at given Julian day.
c It requires some ephemeris files, placed in the 'path' directory.
```

```
c      Argument description:
c CJD_E - Julian Day number representing the Coordinated Universal Time
c      If CJD_E is negative it is assumed that it is -1* (Ephemeris JD).
c clat - observatory conventional geographical latitude (deg).
c clong - observatory conventional geographical longitude (deg).
c height- observatory height above the Earth ellipsoid (m).
c pvo - 6 element array of barycentric vectors (3 for position in km, and
c      3 for velocity in km/s) of the observatory relative to Earth baryc.
c pve - 6 element array of barycentric vectors (3 for position in km,
c      and 3 for velocity in km/s) of the Earth barycenter relative to SSB.
```

```
c More important subroutines called:
c polmot (CJD, Px, Py, UTl_UTC, dpsl, deps)- reads polar motion and UTl data
c topobs (DJl, glat, glong, height, pvo, amst) - returns observer's coord. in 'pvo'
c earthPV (BJD, pve)-returns Earth barycentric position (J2000 frame) in 'pve'
```

-
- [1] P. R. Brady, T. Creighton, C. Cutler, and B. F. Schutz, Phys. Rev. D **57**, 2101 (1998).
 - [2] P. Jaranowski, A. Królak, and B. F. Schutz, Phys. Rev. D **58**, 063001 (1998).
 - [3] M. A. Papa, P. Astone, S. Frasca, and B. F. Schutz, in *Proceedings of the 2nd Workshop on Gravitational Wave Data Analysis*, edited by M. Davier and P. Hello (Éditions Frontières, Paris, 1998), pp. 241–246.
 - [4] M. A. Papa and B. F. Schutz, in *Proceedings of the XXXIVth Rencontres de Moriond: Gravitational Waves and Experimental Relativity*, edited by J. Trân Thanh Vân, J. Dumarchez, S. Reynaud, C. Salomon, S. Thorsett, and J.-Y. Vinet (World Publishers, Hanoi, 2000), pp. 199–205.
 - [5] P. R. Brady and T. Creighton, Phys. Rev. D **61**, 082001 (2000).
 - [6] P. Jaranowski and A. Królak, Phys. Rev. D **61**, 062001 (2000).
 - [7] B. J. Owen, Phys. Rev. D **53**, 6749 (1996).
 - [8] S. D. Mohanty and S. V. Dhurandhar, Phys. Rev. D **54**, 7108 (1996).
 - [9] S. D. Mohanty, Phys. Rev. D **57**, 630 (1998).
 - [10] T. A. Apostolatos, Phys. Rev. D **52**, 605 (1995).
 - [11] P. Astone *et al.*, Phys. Rev. D **65**, 022001 (2002).
 - [12] E. M. Standish, “JPL Planetary and Lunar Ephemerides, DE405/LE405,” IOM 312.F-98-048 (1998).
 - [13] S. Brandt, *Statistical and Computational Methods in Data Analysis* (Springer-Verlag, New York, 1997).
 - [14] J. C. Lagarias, J. A. Reeds, M. H. Wright, and P. E. Wright, SIAM J. Optimization **9**, 112 (1998).
 - [15] J. Middleditch, W. Deich, and S. Kulkarni, in *Isolated Pulsars: Proceedings of the Los Alamos Workshop*, Taos, New Mexico, 1991, edited by C. Ho, R. Epstein, and K. A. Van Riper (Cambridge University Press, Cambridge, England, 1993).
 - [16] H. L. Van Trees, *Detection, Estimation and Modulation Theory* (Wiley, New York, 1969), pt. I.
 - [17] K. D. Kokkotas, A. Królak, and G. Tsebas, Class. Quantum Grav. **11**, 1901 (1994).

- [18] R. Balasubramanian, B. S. Sathyaprakash, and S. V. Dhurandhar, Phys. Rev. D **53**, 3033 (1996).
- [19] P. Astone *et al.*, Phys. Rev. D **47**, 362 (1993).
- [20] P. Jaranowski and A. Królak, Phys. Rev. D **49**, 1723 (1994).
- [21] K. S. Thorne, in *Three Hundred Years of Gravitation*, edited by S. W. Hawking and W. Israel (Cambridge University Press, Cambridge, England, 1987), pp. 330–458.
- [22] M. Montero, Ph.D. thesis, Universitat de Barcelona, 1998.